

Supplementary information:

Enhanced promotion of Ru-based ammonia catalysts by in-situ dosing of Cs

Vahid Shadravan[†], Ang Cao[†], Vanessa J. Bukas[§], Mette K. Grønborg, Christian D. Damsgaard, Zhenbin Wang, Jakob Kibsgaard, Jens K. Nørskov*, and Ib Chorkendorff*

Department of Physics, Technical University of Denmark, 2800 Kongens Lyngby, Denmark

[†] These authors have contributed equally

[§] Present address: Fritz-Haber-Institut der Max-Planck-Gesellschaft, 14195 Berlin, Germany

* Corresponding authors, e-mail: jkno@dtu.dk, ibchork@fysik.dtu.dk

Table S1. Overview of some of the interesting and recently reported catalysts for thermochemical ammonia synthesis.

Catalyst (as named in the ref.)	Testing conditions			Catalyst Performance		Ref.
	Pressure [bar]	Temperature [°C]	WHSV [ml.g ⁻¹ .h ⁻¹]	Activity [mmol.g ⁻¹ .h ⁻¹]	Activity [mmol.gRu ⁻¹ .h ⁻¹]	
Ru(5%)/C_inCs	10	380	48,000	63.7	1274.0	This work
Ru(10%)/C_inCs	10	380	48,000	81.1	811.0	This work
Ru/C_exCs (Cs/Ru = 10)	10	380	48,000	36.1	839.5	This work
Ba-Ru-Li/AC	10	459	62,400	46.3	964.6	1
Li-Ru/(111)MgO	10	400	62,400	33.04	660.8	1
Cs-Ru/(111)MgO	10	400	62,400	22	440.0	1
Ba-Ru/AC	10	400	18,000	8.285	91.0	2
Cs-Ru/MgO	10	400	18,000	12.117	202.0	2
Cs-Ru/r-CeO ₂	10	400	18,000	14.266	356.7	3
Ru/C12A7:e-	10	400	18,000	8.245	206.1	2
K-Ru/r-CeO ₂	10	400	18,000	11.227	280.7	3
Co/CeO ₂ -D-500	10	425	NP	19	NA	4
Ru@CeO ₂ -9	10	425	NP	13.5	544.3	4
Cs-Ru/BaCeO ₃ -a (1.25wt%)	10	425	24,000	14.57	1165.6	5
Ru-Ba/Al ₂ O ₃ -980	10	400	60,000	7.217	144.3	6
Ru-Cs/MgO-MIL	10	400	24,000	19.2	619.4	7
TiH ₂	10	400	66,000	0.7	NA	8
Cr-LiH	10	350	60,000	8.5	NA	9
Mn-LiH	10	350	60,000	6	NA	9
Fe-LiH	10	350	60,000	10.7	NA	9
Co-LiH	10	350	60,000	11.2	NA	9
Ru/Pr ₂ O ₃	10	400	18,000	19.1	382.0	10
K ₂ [Mn(NH ₂) ₄]	10	400	60,000	11.1	NA	11

Ru/Ce _{0.6} Zr _{0.4} O ₂	10	390	18,000	1.7	43.9	12
Ru/Ca ₂ N:e-	10	320	36,000	4	222.2	13
3BaH ₂ -10%Co/CNTs	10	400	60,000	21	NA	14
Ba-Co/C	10	440	160,000	86.4	NA	15
KM1	10	440	160,000	46.8	NA	15
Ba0.35-Fe/C	10	400	53,300	14.4	NA	16
Ba0.35-Co/C	10	400	53,300	22.32	NA	16
LaRuSi after EDTA	10	400	36,000	14.3	NA	17
Co/C12A7:e-	10	400	18,000	4.2	NA	18
Co-Mo/CeO ₂ (NaNaph)	10	400	72,000	3.15	NA	19
Ru/Ca(NH ₂) ₂	10	320	36,000	31.97	319.7	20
Ru/Ba-Ca(NH ₂) ₂	10	340	36,000	57.05	570.5	21
Co/Ba-Ca(NH ₂) ₂	10	380	36,000	24.42	NA	21
Ru/BaO-CaH ₂	10	320	36,000	30.66	306.6	22
Ru/Ti-Ce-S	10	400	36,000	14.58	486.0	23
Mn4N-LiH	10	300	60,000	2.253	NA	24
Mn4N-BaH ₂	10	300	60,000	1.322	NA	24
LaCoSi	10	400	36,000	5.5	NA	25
Ru/3LaN/ZrH ₂	10	400	60,000	12.8	673.7	26
Ni/CeN	10	340	36,000	9	NA	27
Ni/LaN	10	340	36,000	5.3	NA	28
Ru/Ba/LaCeO _x	10	400	72,000	88.1	1762.0	29
Ba ₂ RuH ₆ /MgO *	10	325	60,000	55	NA	30

NA: Not applicable. NP: Not provided.

* This catalyst is tested at different feed composition (H₂/N₂: 2/3) than others. All other catalysts are tested in stoichiometric feed ratio (H₂/N₂: 3/1)

Table S2. Reaction orders for ammonia synthesis over different catalysts.

Catalyst	α (H ₂)	β (N ₂)	γ (NH ₃)	Ref.
Ru/C_inCs	-0.6	1.5	-0.3	This work
Ru/C_exCs	-1.3	1.8	-0.5	This work
Ru/CaH ₂	0.67	0.57	- 1.6	22
Ru/BaO-CaH ₂	0.45	0.47	- 1.3	22
Ru-Cs/MgO	- 0.43	0.99	- 0.12	31
Ru/C12A7:e-	0.97	0.46	- 1.0	2
Ru/Ba-Ca(NH ₂) ₂	0.75	0.96	- 0.92	21
Ru/Ca ₂ N:e-	0.79	0.53	- 1.0	13
Ru/Ca(NH ₂) ₂	0.55	0.53	- 1.5	20
Cr-LiH	0.62	0.43	-1.2	9
Mn-LiH	1.1	0.12	-1.3	9
Fe-LiH	0.88	0.37	-1.3	9
Co-LiH	0.65	0.48	-1.2	9
Ba-Co/C	2.3	1.2	-1.6	16
Ba-Fe/C	1.2	0.9	-0.9	16
KM1	2.2	0.9	-1.5	16

Table S3. Relative loading of Cesium in different in situ and ex situ promoted catalysts measured by ICP-MS.

Catalyst	Cs loading (wt%)	Cs/Ru (atom/atom)
Ru/C_exCs (Cs/Ru=1)	11 ± 0.2	~ 1
Ru/C_exCs (Cs/Ru=2.5)	32 ± 1.5	~ 3
Ru/C_exCs (Cs/Ru=10)	43 ± 0.5	~ 8
Ru(10%)/C_inCs	53 ± 1.1	~ 8

Table S4. Average particle size of in situ and ex situ catalysts measured by TEM.

Catalyst	Average particle size (nm)
Ru/C_exCs (Cs/Ru=2.5)	3.0 ± 1
Ru(10%)/C_inCs	10 ± 4

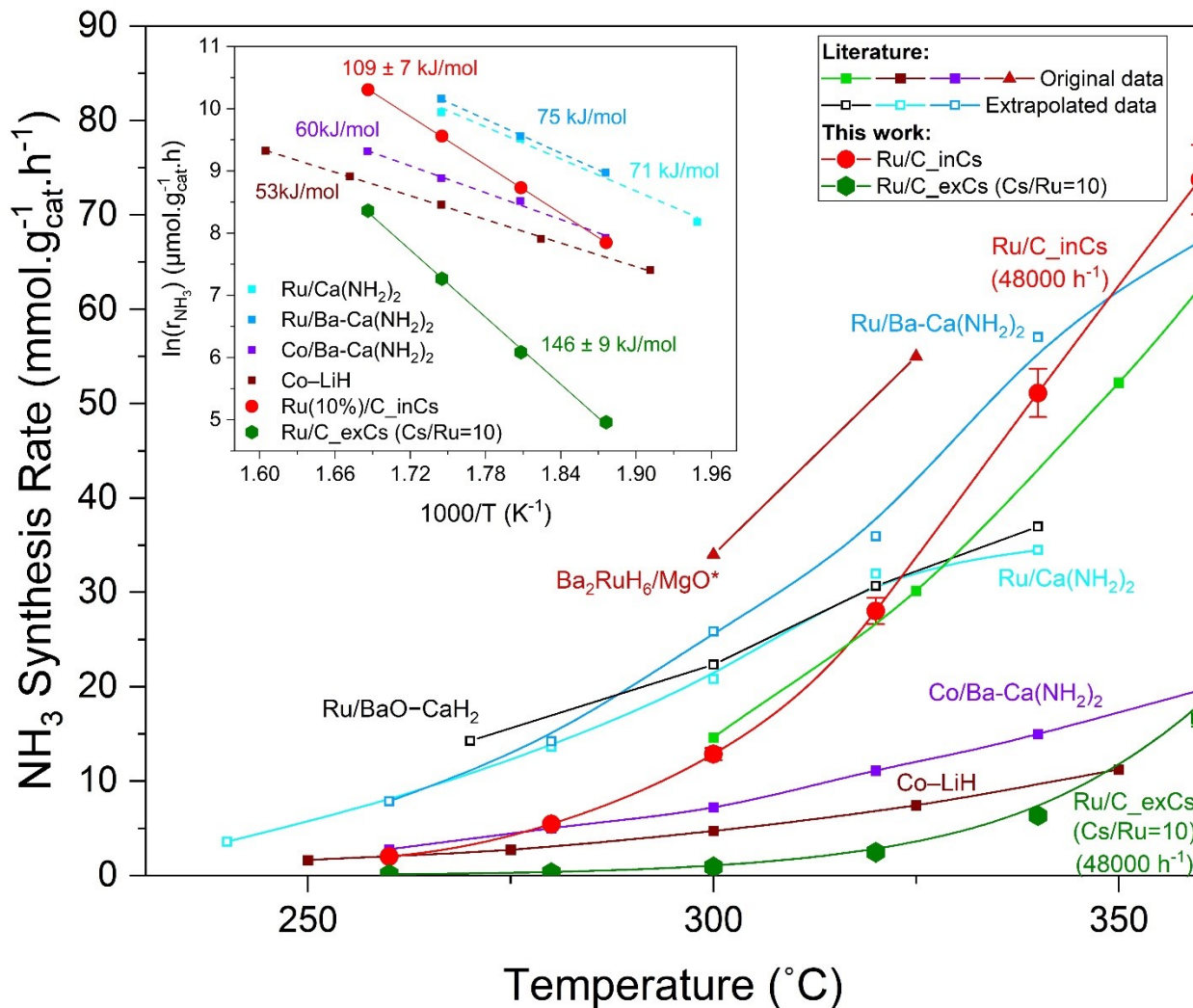


Fig. S1 Overview of some of the most recent and promising catalysts reported for thermochemical ammonia synthesis^{9,20–22,29,30}. Most of data points (filled symbols) are extracted from original references based on the following conditions: Pressure = 10 bar, $H_2/N_2 = 3$. The open symbols are estimated values (at 10 bar) based on the original data reported at lower pressures. The data point with * symbol is tested at a different feed composition ($H_2/N_2: 2/3$)

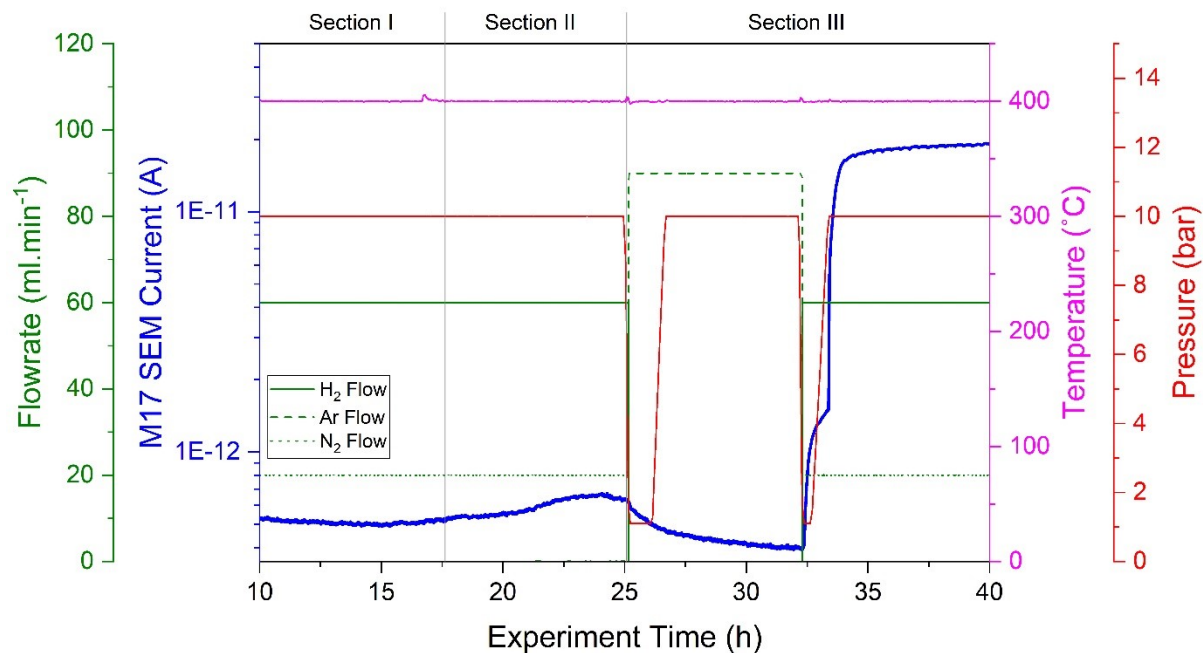


Fig. S2 Ammonia synthesis experiment over 0.1 g Ru/C. Section I: feed stream bypassing Cs-based trap; Section II: feed stream passing through Cs-based trap; Section III: *in situ* dosing of Cs in to the reactor (Cs-dosing in Ar flow started at around 27 h).

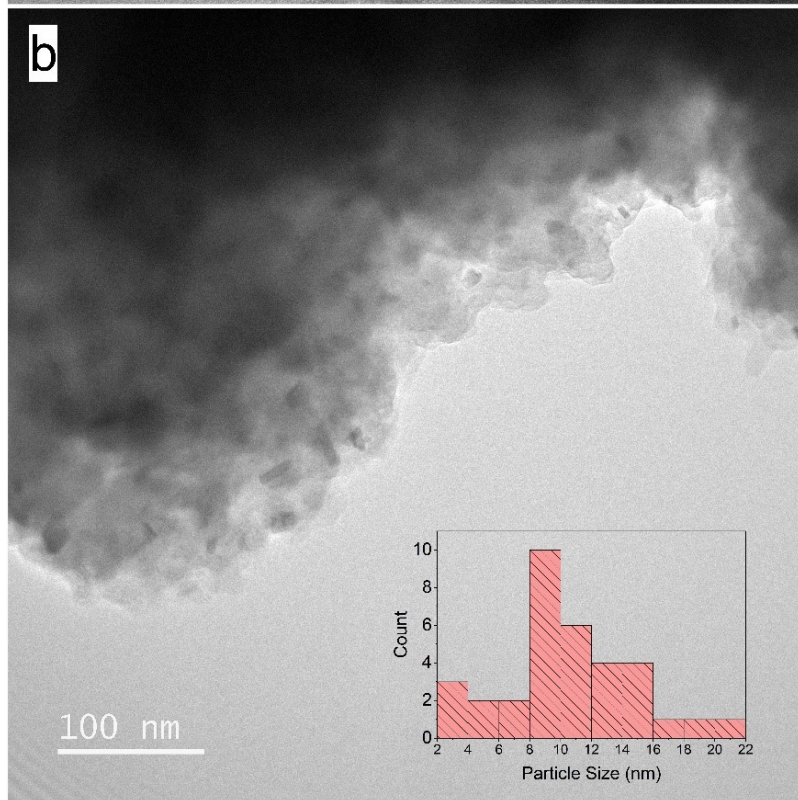
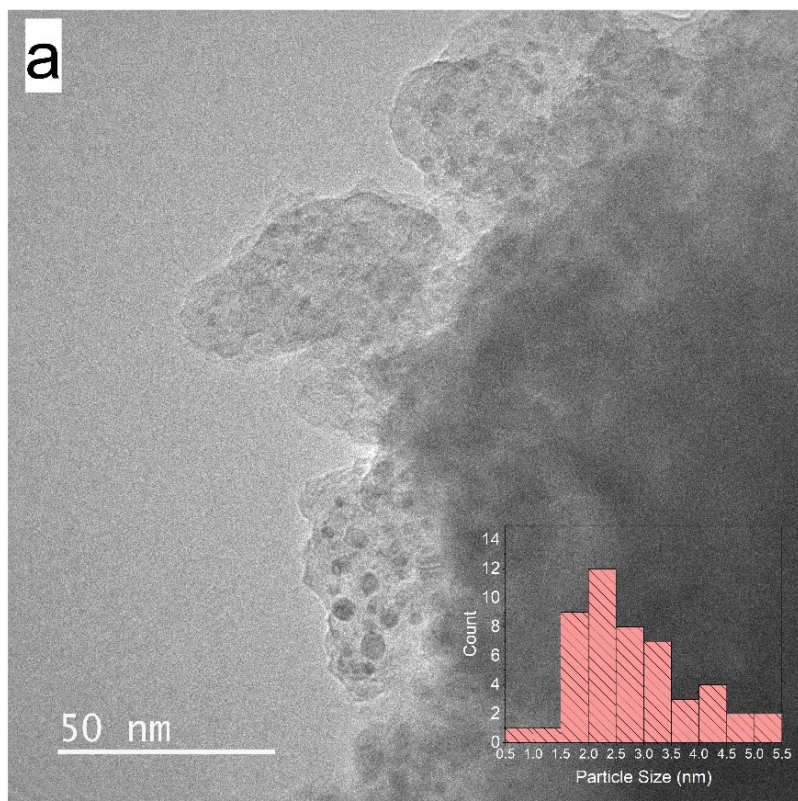


Fig. S3 TEM images of **(a)** Ru/C_exCs (Cs/Ru=2.5), and **(b)** Ru(10%)/C_inCs catalysts.

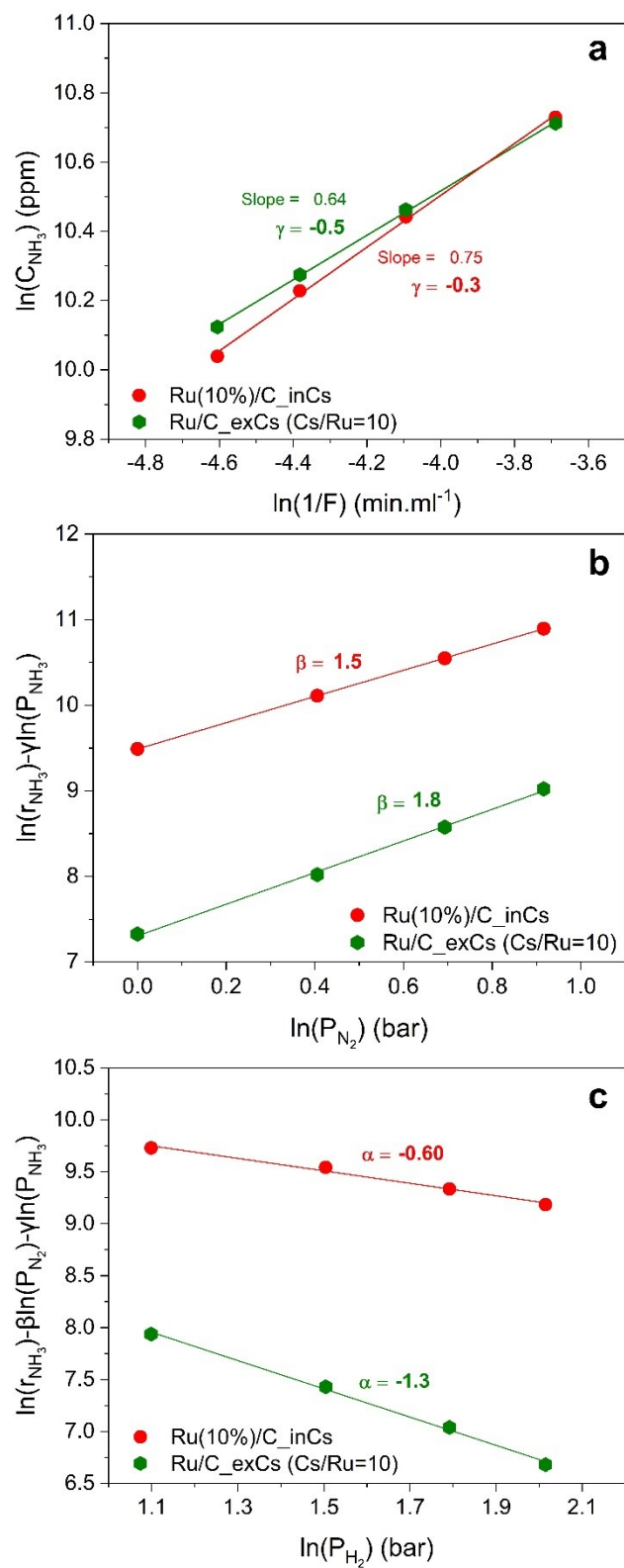


Fig. S4 Reaction order measurements for Ru/C_inCs and Ru/C_exCs.

The performance of *in situ* promoted catalyst in the presence of water

To add a controlled concentration and known amount of water to the feed stream over a period during some experiment, a U-tube was filled with CuO powder (99.99% trace metals basis, Sigma-Aldrich). The U-tube was installed in the feed stream before the reactor with the possibility of being by-passed. The CuO powder was heated to approximately 250 °C. In the period of water addition, the feed stream was passing through the U-tube and then entering the reactor. The amount of CuO was adjusted so the produced water was in excess of the dosed metallic Cs.

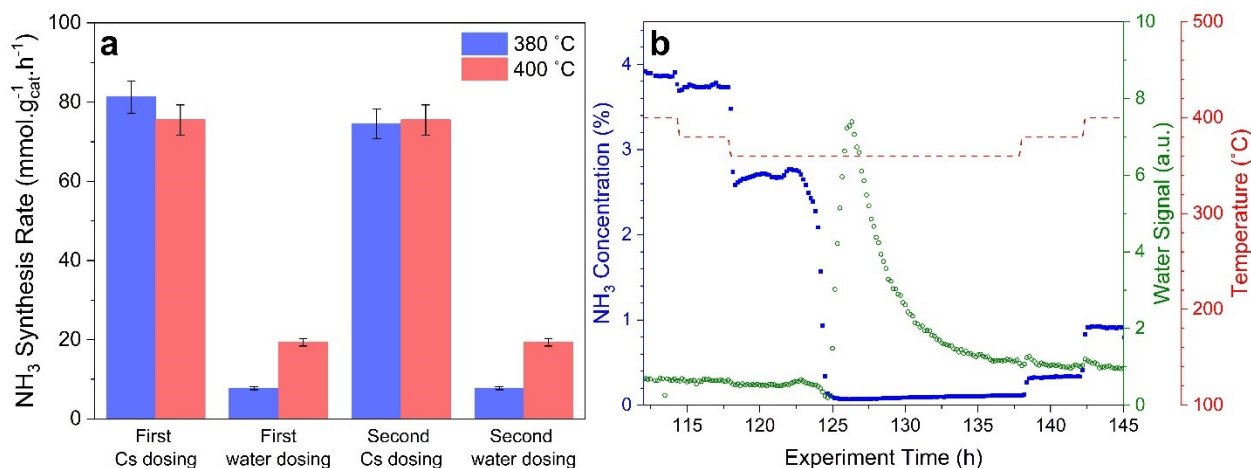


Fig. S5 (a) Comparison of ammonia synthesis rate after two cycles of *in situ* Cs dosing and H₂O dosing over the same Ru/C. **(b)** Changes of produced ammonia concentration over an *in situ* Cs promoted Ru/C before and after introducing small amount of water into the reactants stream.

A freshly loaded Ru/C was *in situ* dosed with metallic Cs vapor to reach its maximum activity. Then, a small amount water was dosed into the reactor and the produced ammonia concentration was monitored. The ammonia synthesis activity was dropped after the injection of water into the reactor and started to after a few hours until it reached a fairly stable level. However, the activity after water dosing could not reach to same level as before. The water-dosed catalyst was then re-dosed with fresh metallic Cs. Interestingly, the H₂O dosed catalyst from the first cycle was able to gain high activity (close to the values after first Cs-dosing) by re-dosing fresh Cs vapor over the second Cs dosing cycle (**Fig. S4a**). **Fig. S4b** shows the changes in ammonia concentration before (experiment time: 112-125 h) and after (experiment time: 138-145 h) the second water dosing step (experiment time: 125-138 h). It is clear that the ammonia synthesis activity of a freshly promoted Ru/C with Cs vapor significantly decreases by introducing water to the catalyst.

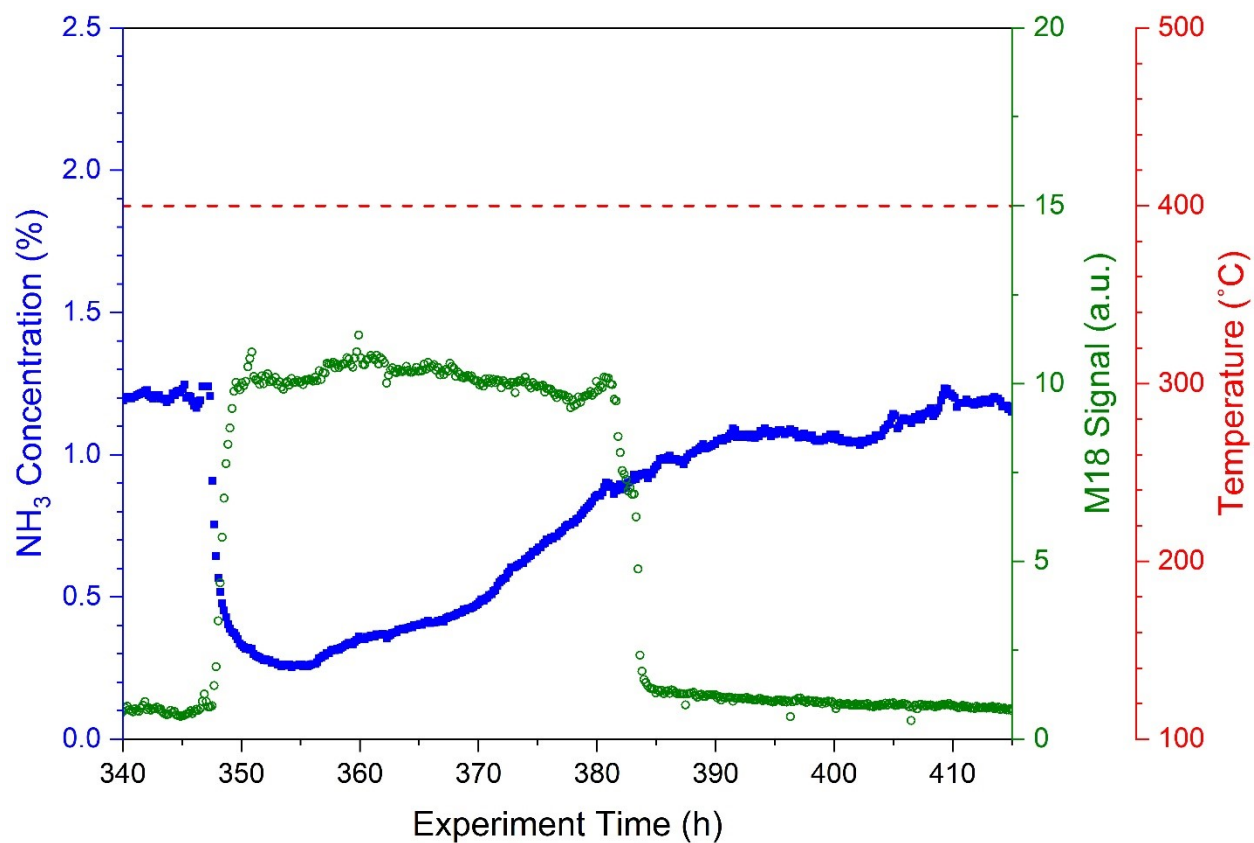


Fig. S6 Performance of Ru/C_inCs H₂O dosed catalyst in presence of H₂O for several hours (continuation after 2nd H₂O dosing step in effect of water experiment).

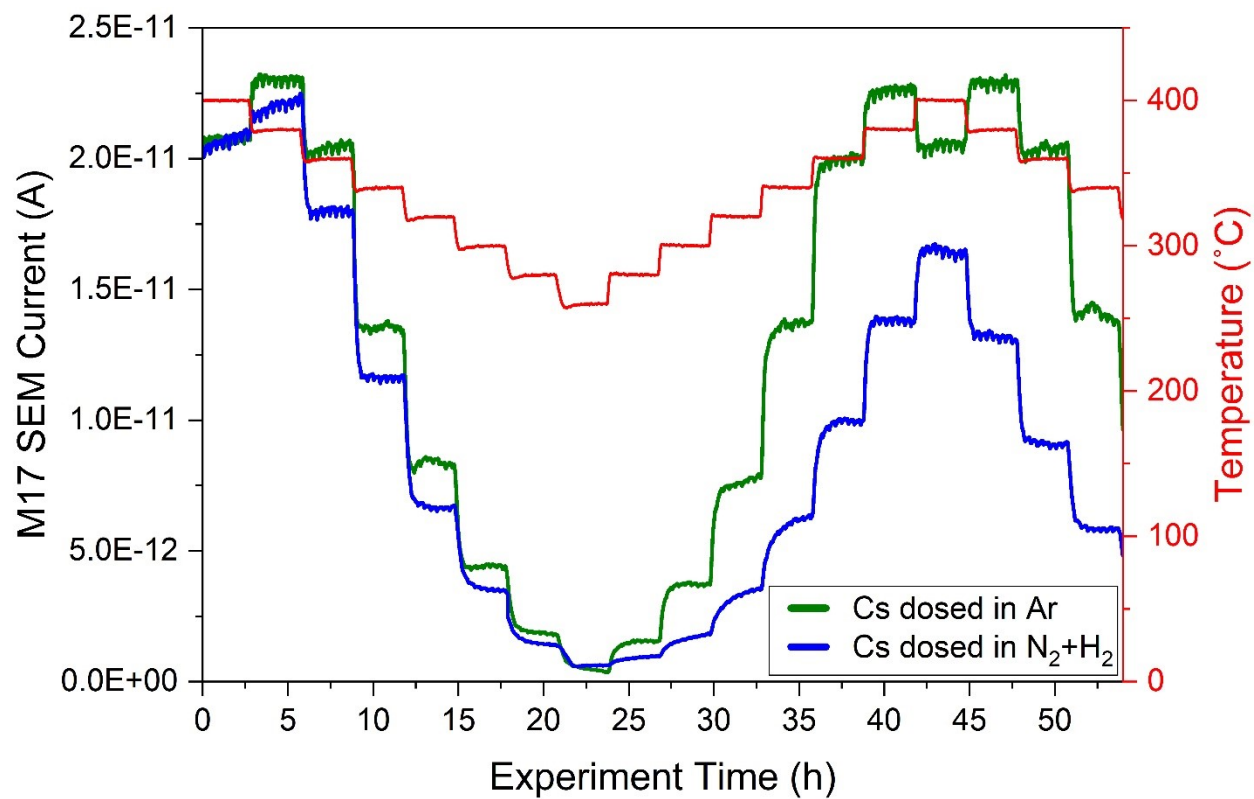


Fig. S7 Comparing the performance of in situ Cs promoted Ru/C catalyst when Cs dosing was done in different gas stream (in Ar and in N₂+H₂ mixture).

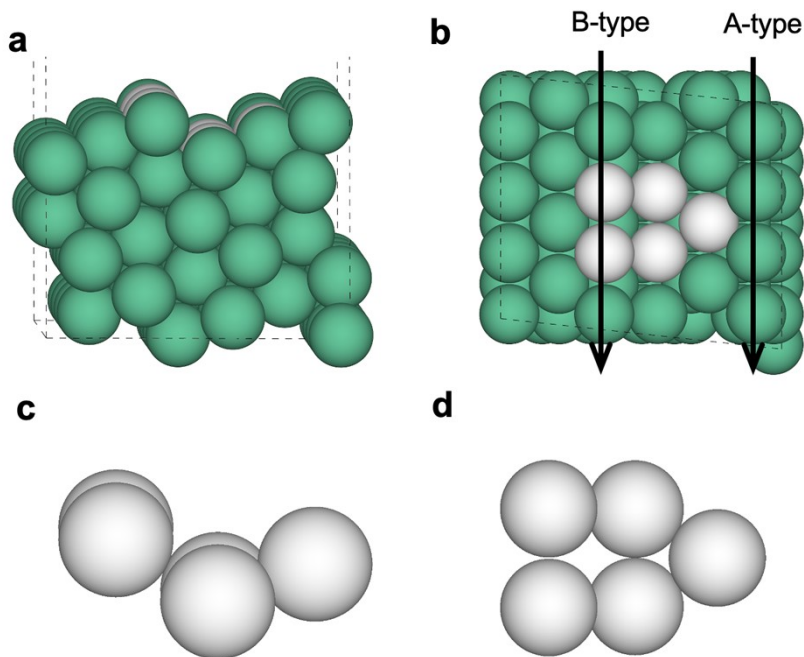


Fig. S8 The side and top views of the Ru($10\bar{1}5$) surface (a-b) and the B5-sites(c-d). Green spheres represent Ru atoms. The Ru atoms on the B5-sites are labeled in grey.

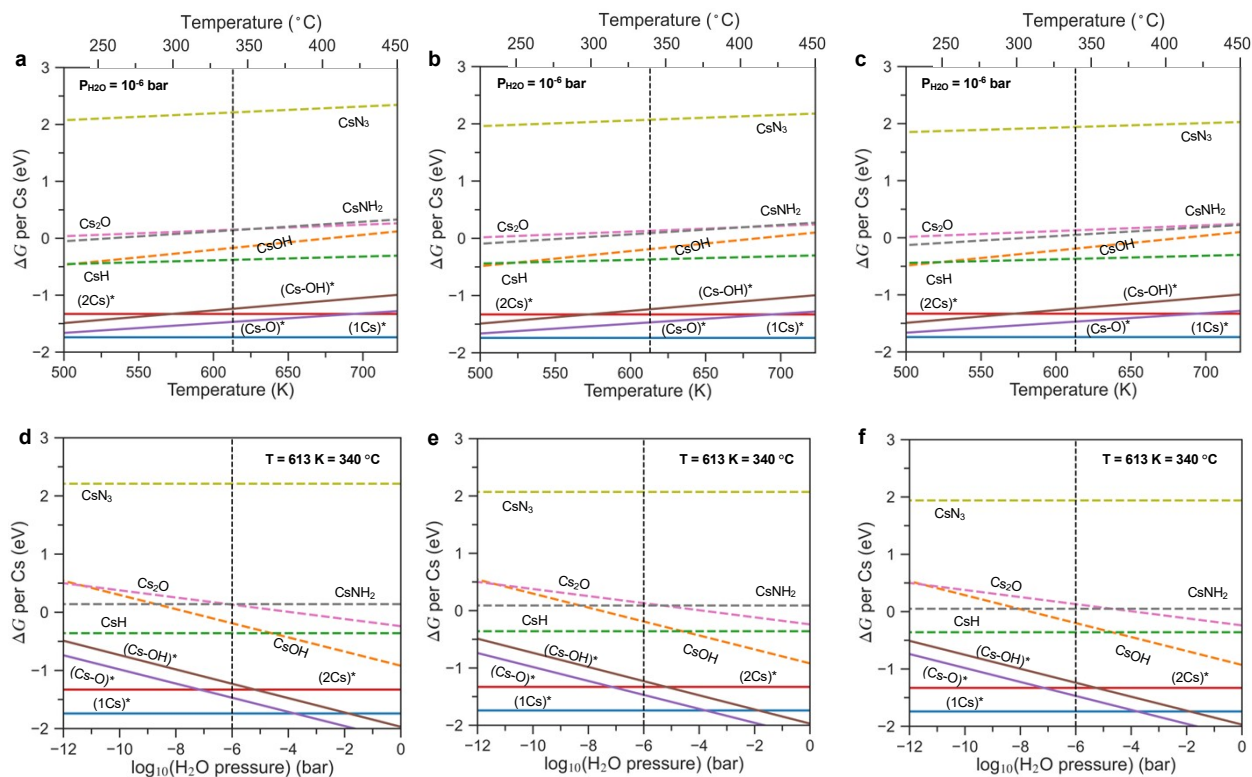


Fig. S9 The phase diagrams of Cs promoted Ru in equilibrium with its oxides, hydroxides and, hydrides, amides and nitrides under reaction conditions as a function of temperature (panels a, b, and c) and H_2O pressure (panels d, e, and f). Three different N_2 conversion values were used in these calculations: 2% (panels a and d), 5% (panels b and e), and 10% (panels c and f).

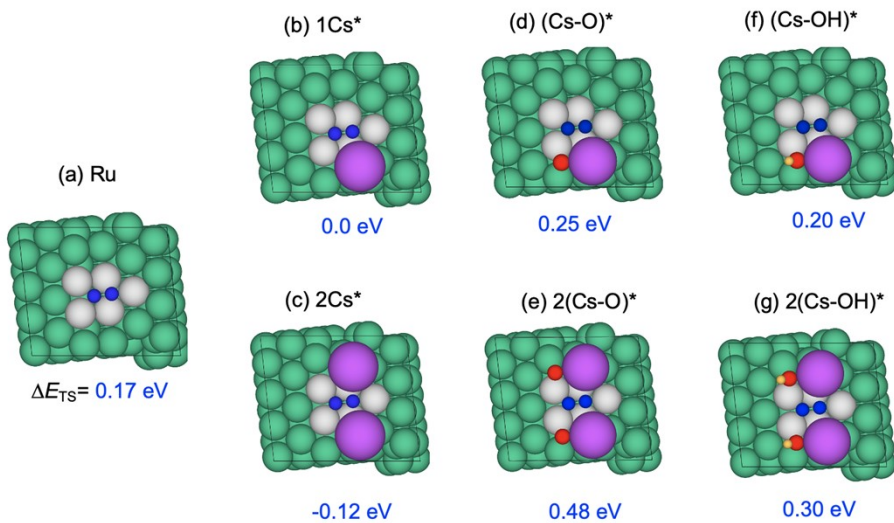


Fig. S10 The calculated N_2 dissociation energies (ΔE_{TS} , labeled in blue number below the configurations) on pristine Ru(a), Cs* doped Ru (b, e), (Cs-O)* doped Ru(c, f) and (Cs-OH)* doped Ru(d, g). Green, purple, red, yellow, and blue spheres represent Ru, Cs, O, H, and N atoms. The Ru atoms on the B5-sites are labeled in grey.

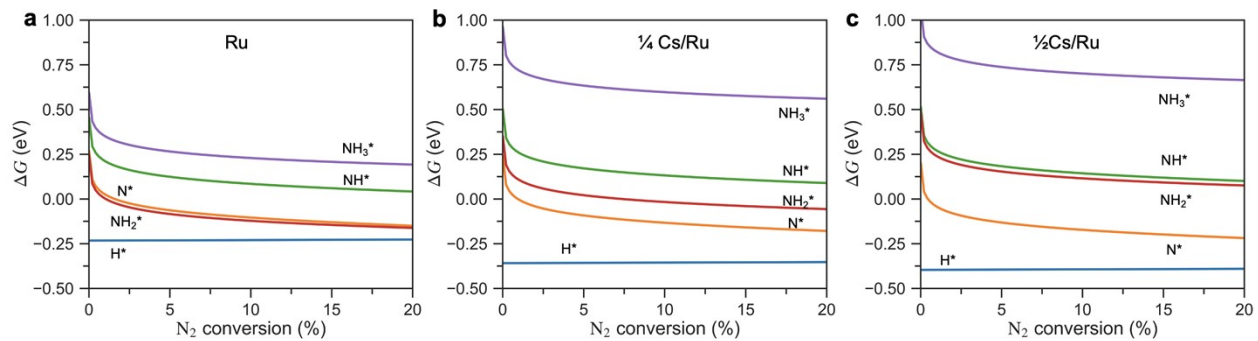
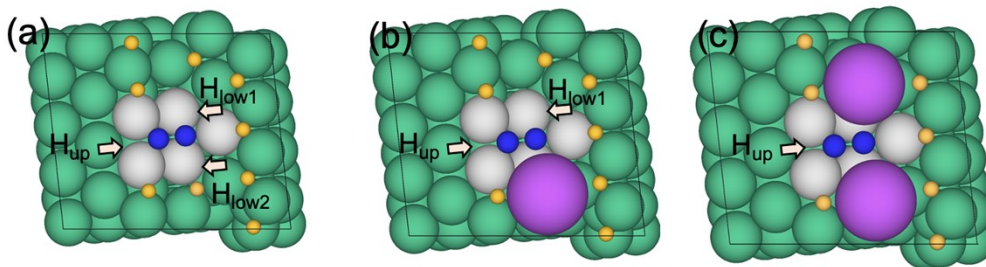


Fig. S11 Phase diagram of H^* and NH_x^* ($x=0, 1, 2$) adsorption energies on (a) Ru, (b) $1/4$ Cs/Ru and (c) $1/2$ Cs/Ru surfaces at $T = 613$ K, $P = 10$ bar, $H_2:N_2=3:1$.

Table S5 Differential electronic (ΔE_H) and free (ΔG_H) binding energies of H^* on the Ru, $\frac{1}{4}$ Cs/Ru and $\frac{1}{2}$ Cs/Ru surfaces at $T = 613$ K, $P_{H_2} = 7.15$ bar.

H* number	Ru		$\frac{1}{4}$ Cs/Ru		$\frac{1}{2}$ Cs/Ru	
	ΔE_H (eV)	ΔG_H (eV)	ΔE_H (eV)	ΔG_H (eV)	ΔE_H (eV)	ΔG_H (eV)
1	-0.54	-0.24	-0.67	-0.36	-0.71	-0.40
2	-0.57	-0.27	-0.64	-0.33	-0.68	-0.38
3	-0.56	-0.26	-0.66	-0.36	-0.73	-0.43
4	-0.56	-0.26	-0.61	-0.31	-0.69	-0.38
5	-0.53	-0.23	-0.54	-0.24	-0.53	-0.23
6	-0.56	-0.26	-0.59	-0.29	-0.58	-0.28
7	-0.51	-0.21	-0.46	-0.16	-0.46	-0.16
8	-0.51	-0.20	-0.52	-0.22	-0.51	-0.20
9	-0.42	-0.12	-0.41	-0.11		
10	-0.41	-0.10	-0.41	-0.10		
11	-0.40	-0.10				
12	-0.38	-0.08				

Table S6 Calculated electronic energies and free energies for N₂ dissociation on pristine Ru, ¼ Cs/Ru and ½ Cs/Ru surface at T = 613 K, P_{H₂} = 7.15 bar, P_{N₂} = 2.375 bar (N₂ conversion = 5%). The topmost images depict the configuration of N-N* transition states on pristine Ru (a), H* covered ¼ Cs/Ru (b) and H* covered ½ Cs/Ru surface. Green, purple, blue and white spheres represent Ru, Cs, N, and H, respectively. The Ru atoms on the B5-sites are labeled in grey. H_{up} and H_{low} mean the removed H atoms on step sites and lower step sites, respectively.



	Ru		¼ Cs/Ru		½ Cs/Ru	
	$\Delta E(\text{eV})$	$\Delta G(\text{eV})$	$\Delta E(\text{eV})$	$\Delta G(\text{eV})$	$\Delta E(\text{eV})$	$\Delta G(\text{eV})$
$\Delta E_{\text{H}_{\text{up}}}$	-0.56	-0.26	-0.61	-0.31	-0.69	-0.38
$\Delta E_{\text{H}_{\text{low1}}}$	-0.40	-0.10	-0.41	-0.10		
$\Delta E_{\text{H}_{\text{low2}}}$	-0.38	-0.08				
$\Sigma \Delta E_{\text{H}}$	-1.35	-0.44	-1.02	-0.41	-0.69	-0.38
$E_a, \text{N}_2 \text{ diss}$	0.38	1.30	0.22	1.14	0.12	1.05
$E_a, \text{apparent}$	1.72		1.24		0.80	
G_a		1.74		1.55		1.43

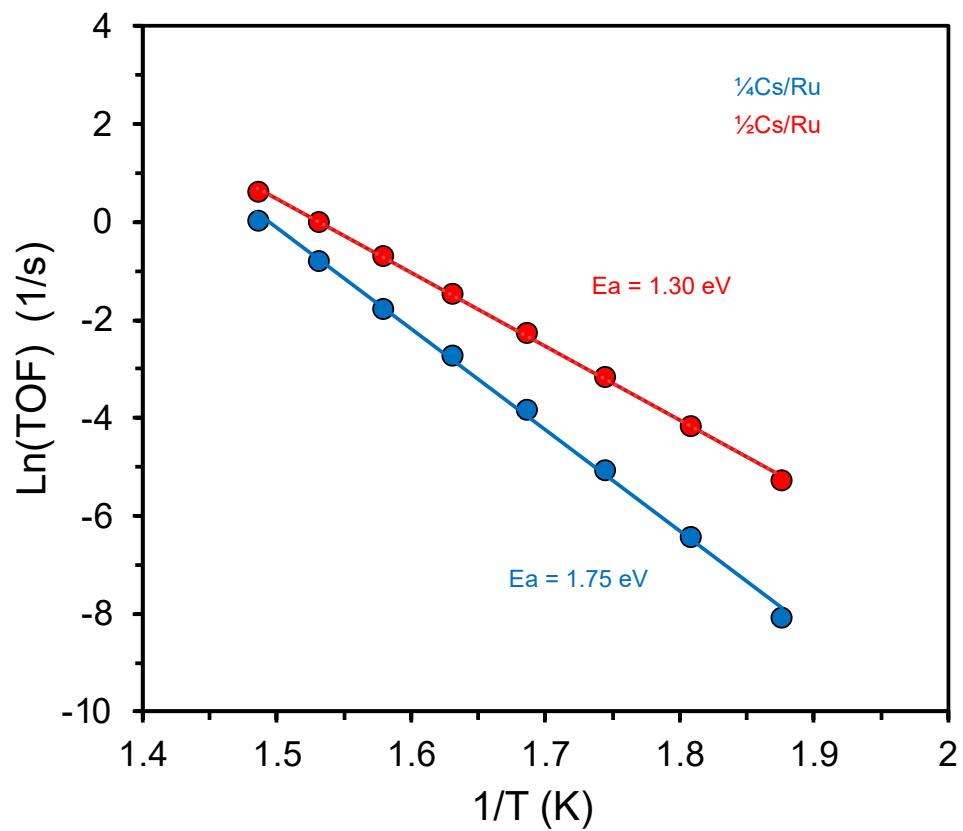


Fig. S12 Calculated apparent barriers and rates on $\frac{1}{4}$ Cs/Ru and $\frac{1}{2}$ Cs/Ru by kinetic analysis. Reactions are $P_{\text{total}} = 10\text{bar}$, $\text{H}_2:\text{N}_2=3:1$ and the N_2 conversion is 2%.

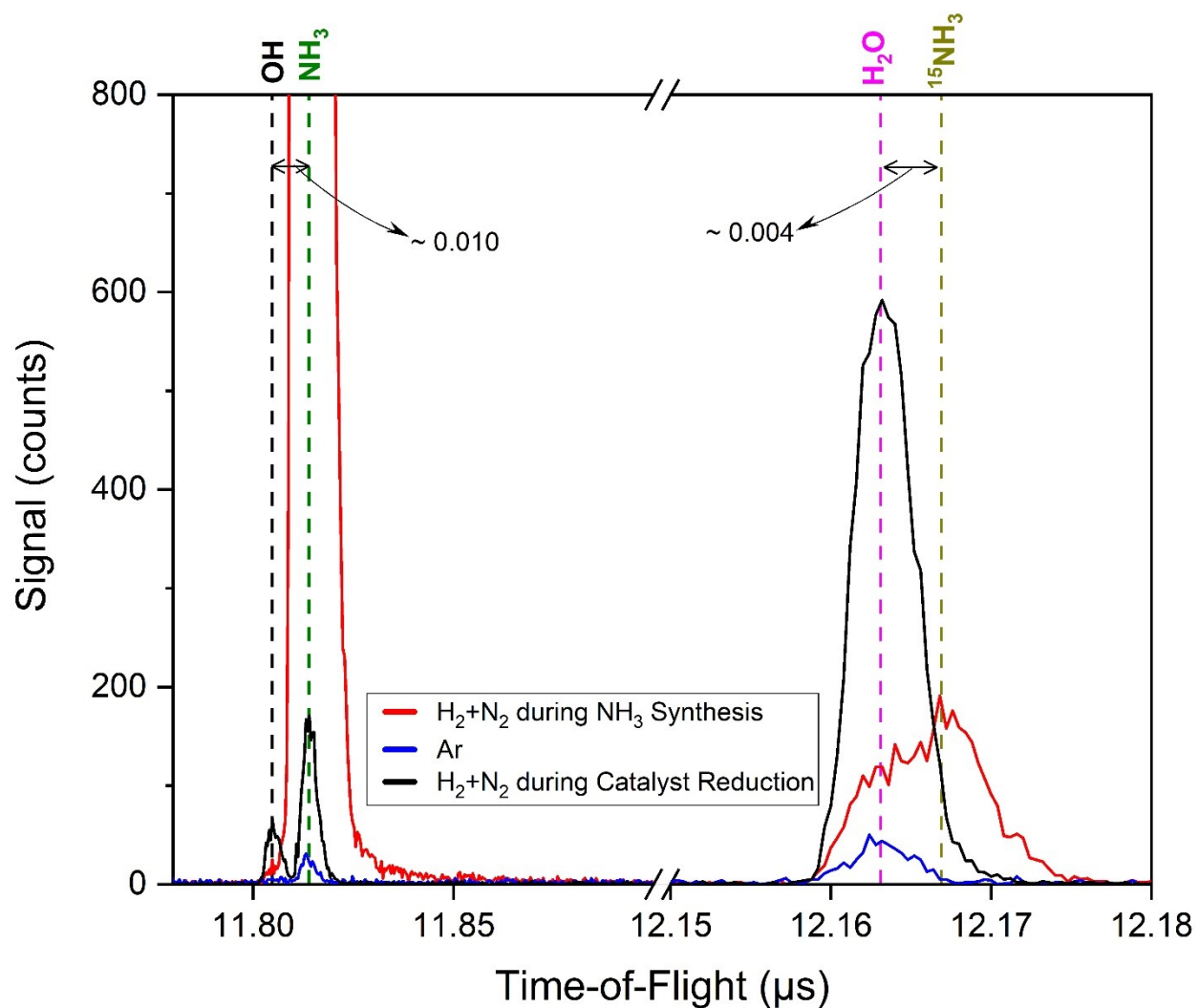


Fig. S13 Details of Time-of-Flight Mass Spectrometer (ToF-MS) spectra at mass 17 and 18. The high mass resolution of ToF-MS allows us to distinguish between species that have very close masses (such as OH and NH₃, or H₂O and ¹⁵NH₃).

XRD

The collected XRD patterns of *in situ* and *ex situ* promoted catalysts were analyzed using HighScore Plus and reference pattern from Inorganic Crystal Structure Database (ICSD). Both *in situ* and prompted catalysts were matched with cesium hydrogen carbonate (CsHCO_3) reference patterns. This is most probably due to the reaction of metallic Cs on the samples with H_2O and CO_2 in the ambient air to form CsHCO_3 .

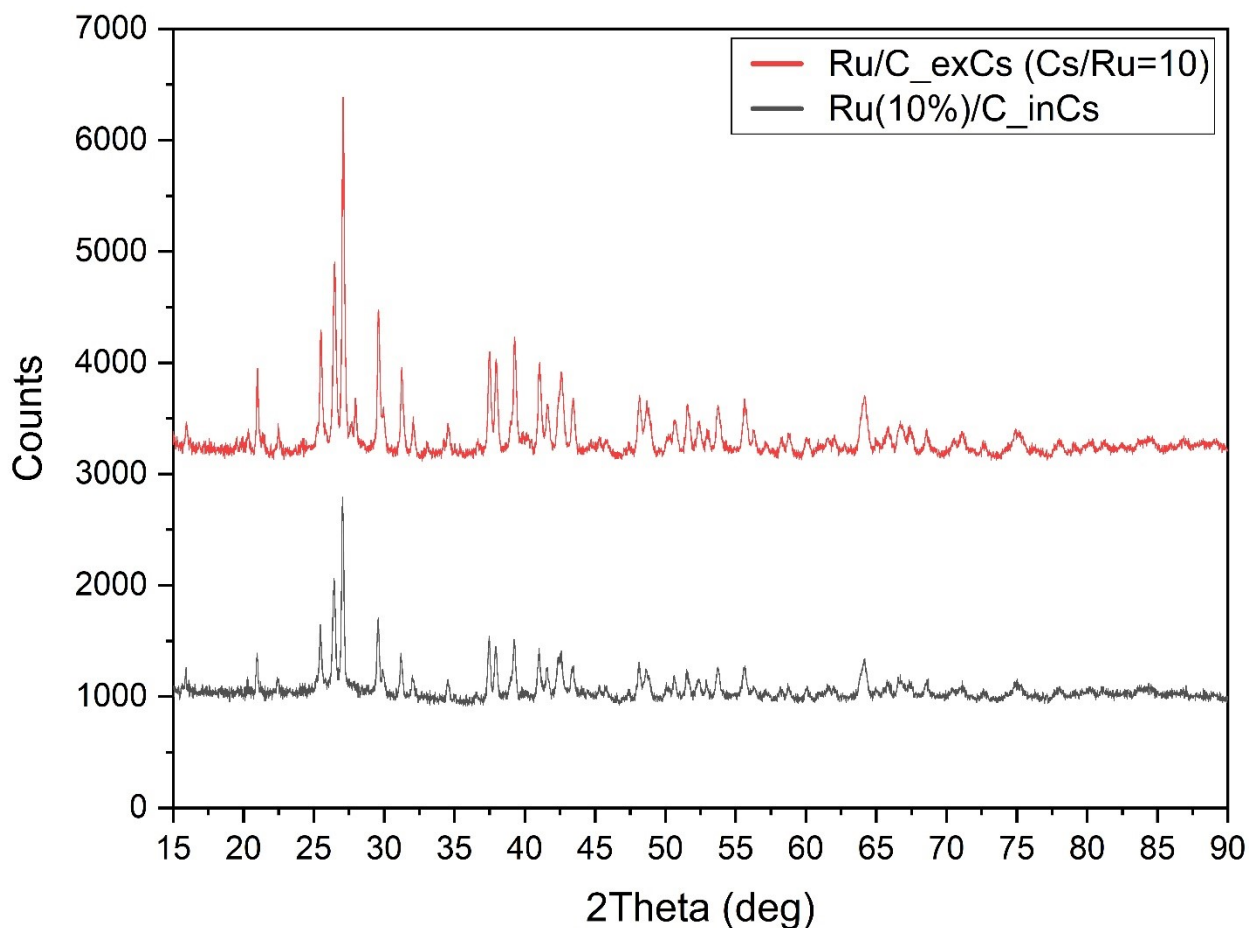
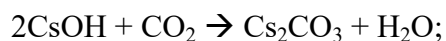


Fig. S14 XRD patterns of *in situ* and *ex situ* promoted catalysts.

XPS analysis

XPS spectra of the un-promoted and *in situ* promoted Ru/C catalysts were collected (details in Methods section). The *in situ* promoted XPS samples were prepared in two different environments: in ambient air and in Ar glovebox (named as in air and in glovebox, respectively). The un-promoted sample was prepared in ambient air (named as Fresh). The in air prepared samples were transferred to the Ar glovebox after being pre-heated. All the samples were transferred to the XPS chamber with a UHV compatible transfer arm to avoid any exposure to ambient air while being transferred. The XPS spectra were collected for all samples (Layer 0), then the samples were sputtered using an Ar-sputter gun for four times and after each sputtering XPS spectra were collected (Layers 1-4).

Fig. S15 shows the survey scans for all three samples (layer 0). The spectra of the *in situ* promoted samples are dominated by Cs features. **Fig. S16-17** present the detailed scans of carbon, ruthenium, cesium, and oxygen. The Ru features (Ru3d and Ru3p) were observed for all three samples. For the Ru(10%)/C Fresh and Ru(10%)/C_inCs in air samples the Ru peaks shifted to smaller binding energies (towards smaller oxidation state) after the first sputtering, which is most probably due to the known reduction effect of Ar-sputtering. The sputtered layers are well aligned and no shift was observed from layer 1 to 4. The similar effect was seen for the Cs features of the promoted samples. The Cs peaks are shifted to higher binding energies after sputtering which indicates that they were reduced because of the Ar-sputtering.

The carbon peak of Ru(10%)/C Fresh and Ru(10%)/C_inCs in air samples are fairly similar to each other (around 284.5 eV), while the Ru(10%)/C_inCs in glovebox sample has two peaks for carbon. The extra carbon peak of Ru(10%)/C_inCs in glovebox sample can be assigned to carbonate species. The formation of carbonate species on reactive metals such as Cs is anticipated in our glovebox atmosphere and we have seen the same effect on Li foils using the same transfer technique. Unfortunately, this shows that even avoiding air exposure and using inert atmospheres (such as Ar) is not enough to evaluate and understand the actual oxidation states of our catalysts during the reaction (an ideal system would be a high pressure reactor with the possibility of direct transfer of the sample to a UHV chamber for surface characterization such as XPS). However, we could still see that the sample transferred in air has a higher oxidation state for Cs compared to the transferred in Ar (see **Fig S.19 b** and **c**).

Two sets of XPS measurements were done for the Ru/C_exCs (Cs/Ru=10): before and after reaction testing. The after-reaction sample was first unloaded from the reactor in an Ar glovebox, then both before and after samples were prepared in the glovebox. Both samples were transferred to the XPS instrument in air. The XPS spectra of these two samples are fairly similar to each other and the *in situ* samples (especially the in air prepared one), this can be most probably due to the highly reactive nature of the samples which are easily oxidized outside the reactor.

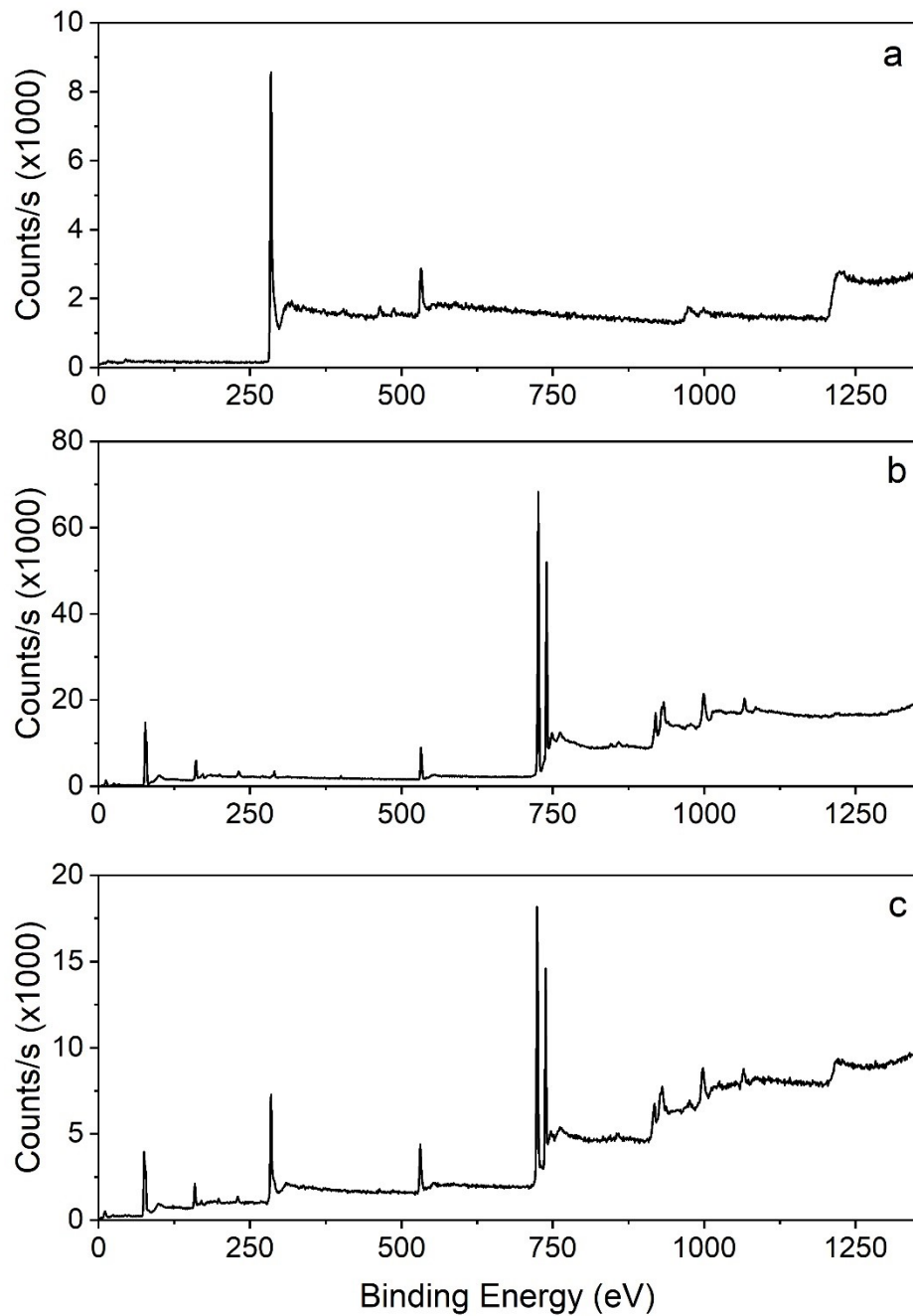


Fig. S15 Survey XPS spectra of (a) Ru(10%)/C fresh, (b) Ru(10%)/C_inCs prepared in ambient air, and (c) Ru(10%)/C_inCs prepared in Ar glovebox.

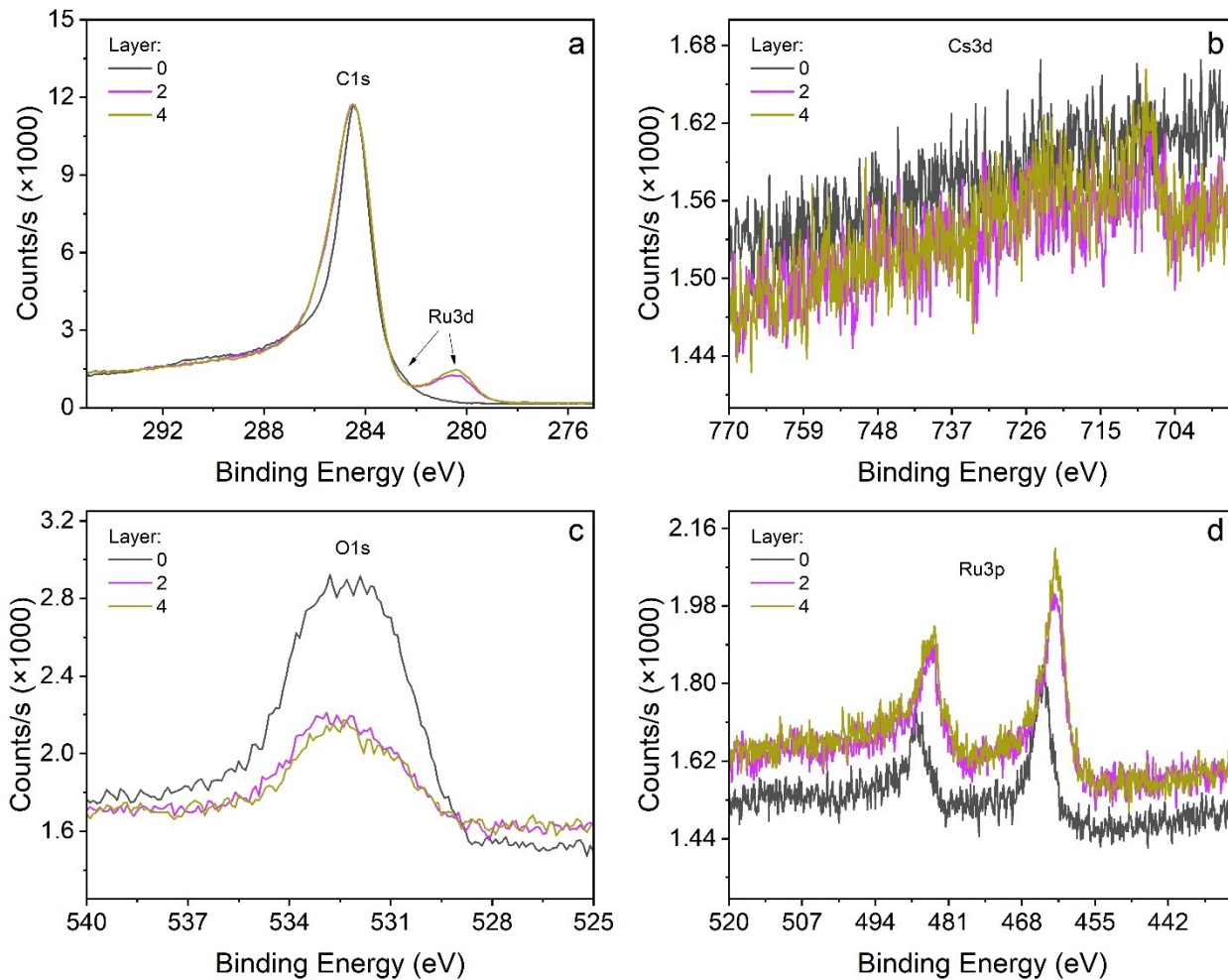


Fig. S16 Detailed XPS spectra of the Ru(10%)/C fresh.

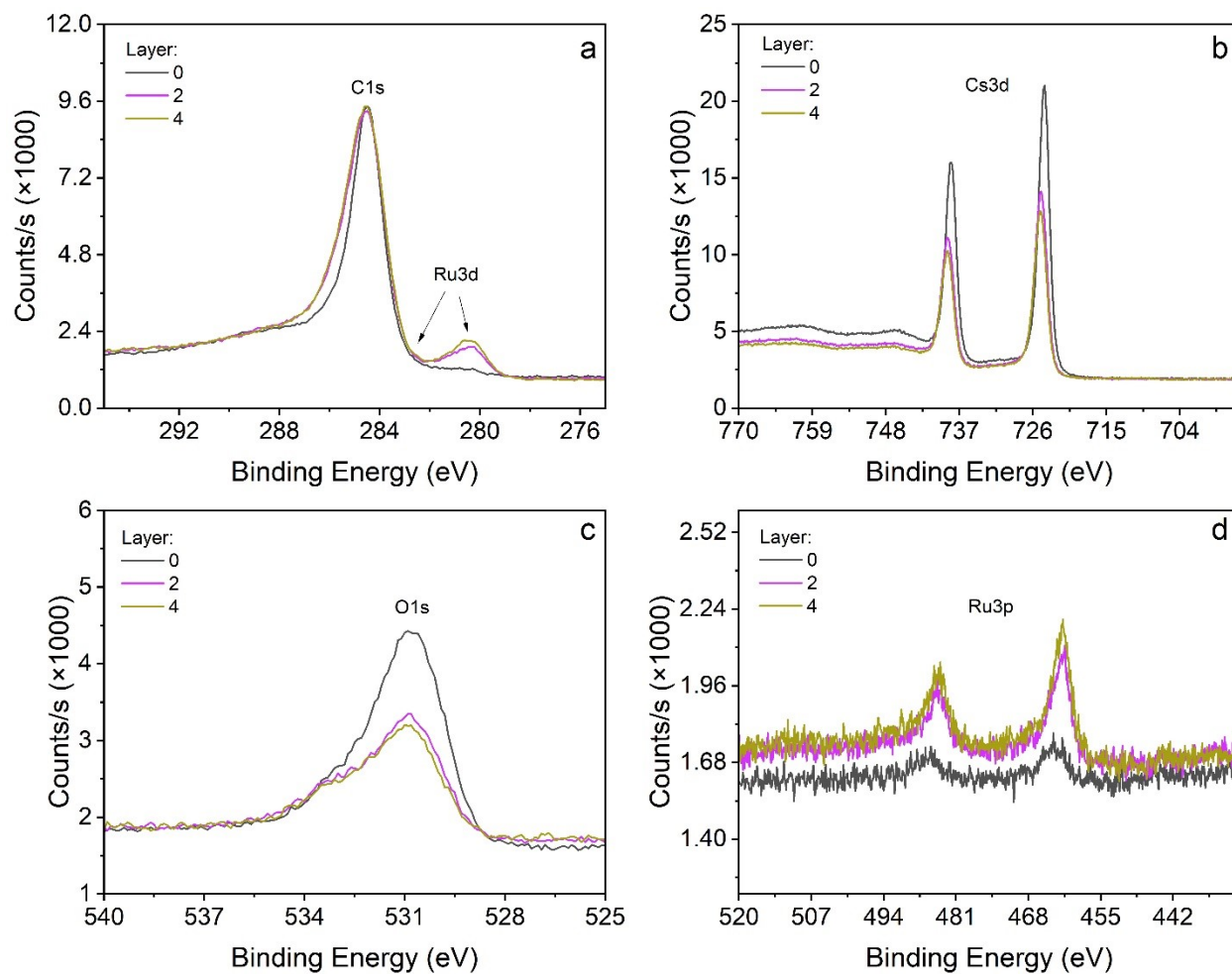


Fig. S17 Detailed XPS spectra of the Ru(10%)/C_{in}Cs prepared in ambient air.

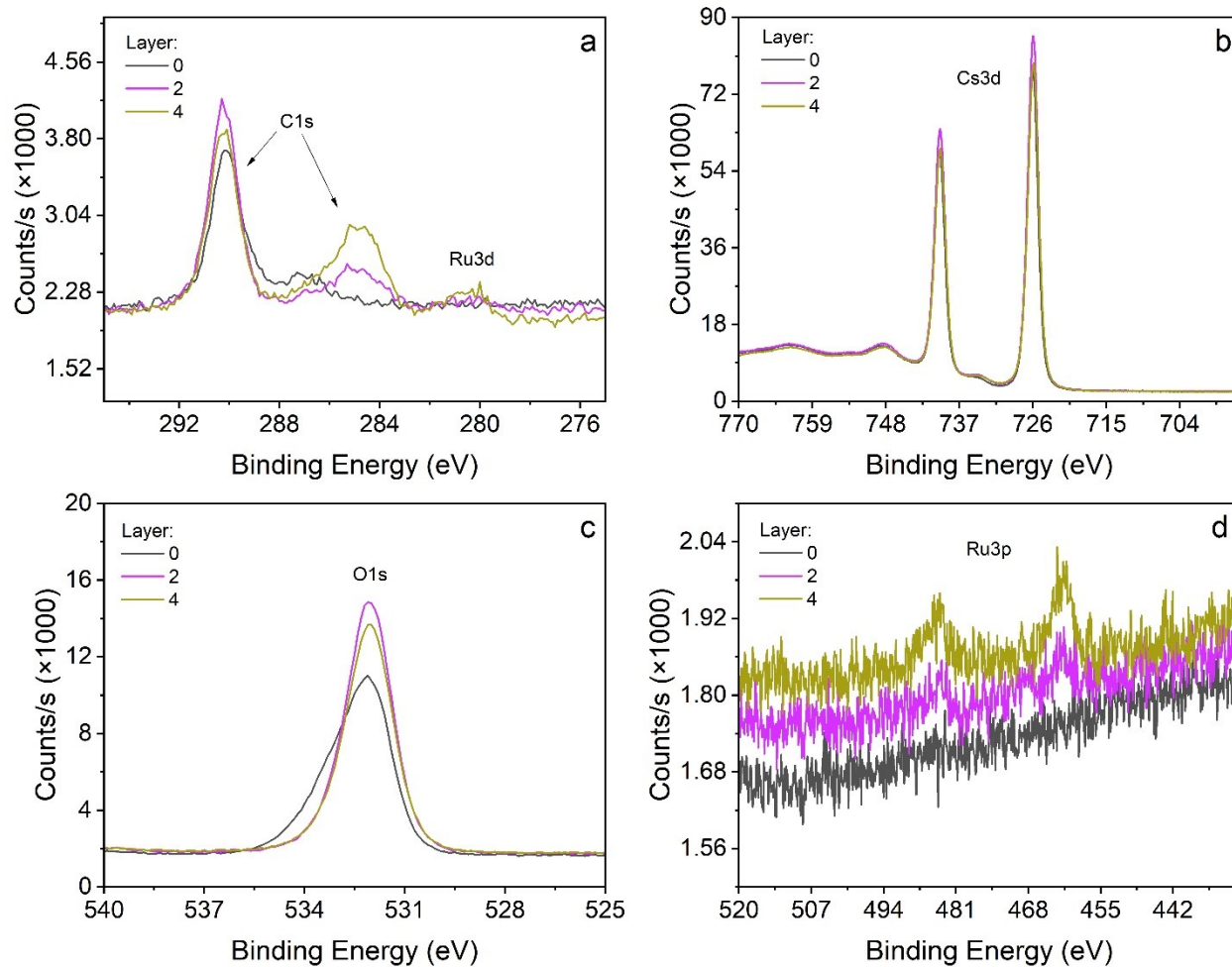


Fig. S18 Detailed XPS spectra of the Ru(10%/C_{in}Cs prepared in Ar glovebox.

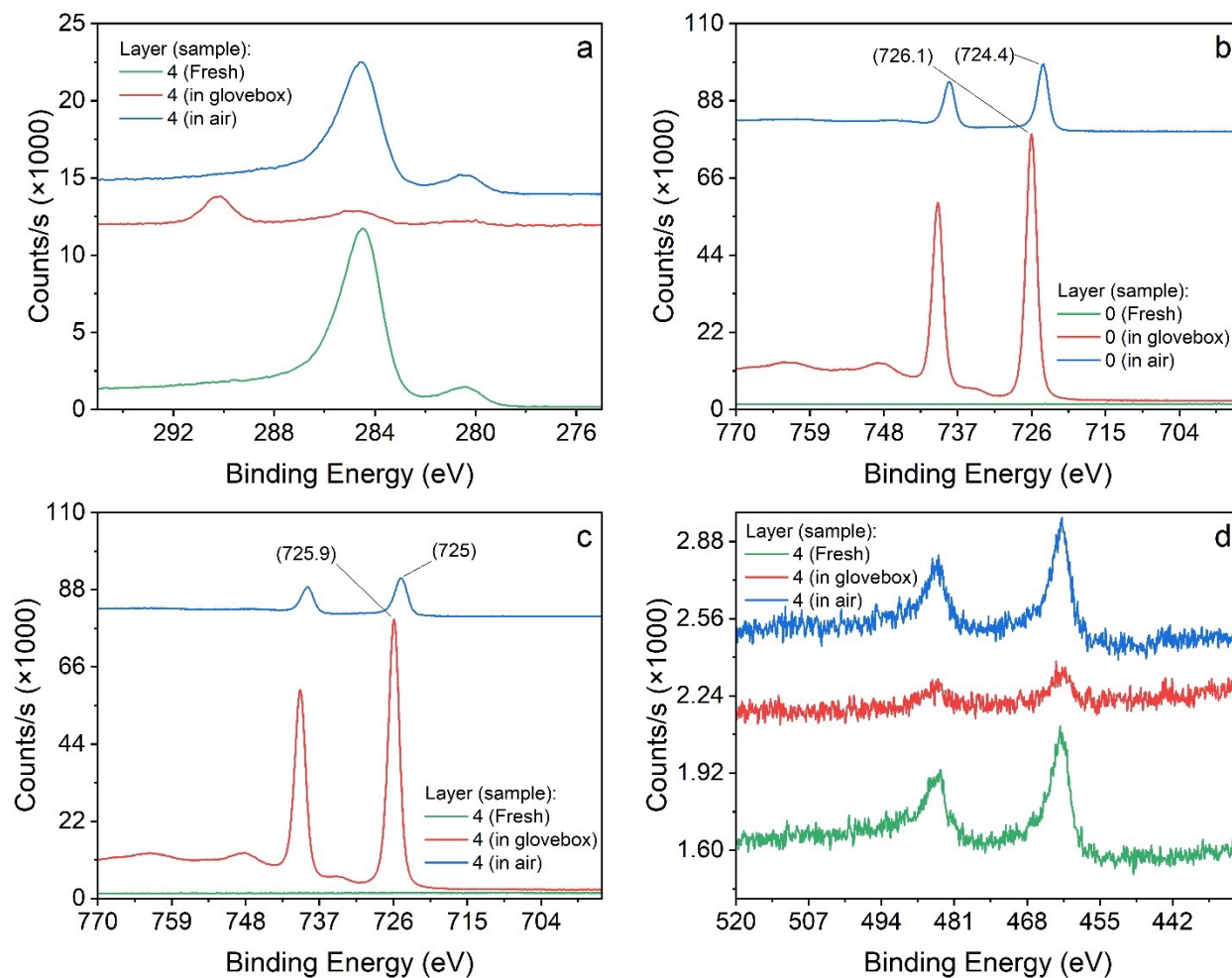


Fig. S19 Stacked detailed XPS spectra of Ru(10%)/C fresh, Ru(10%)/C_inCs prepared in ambient air, and Ru(10%)/C_inCs prepared in Ar glovebox.

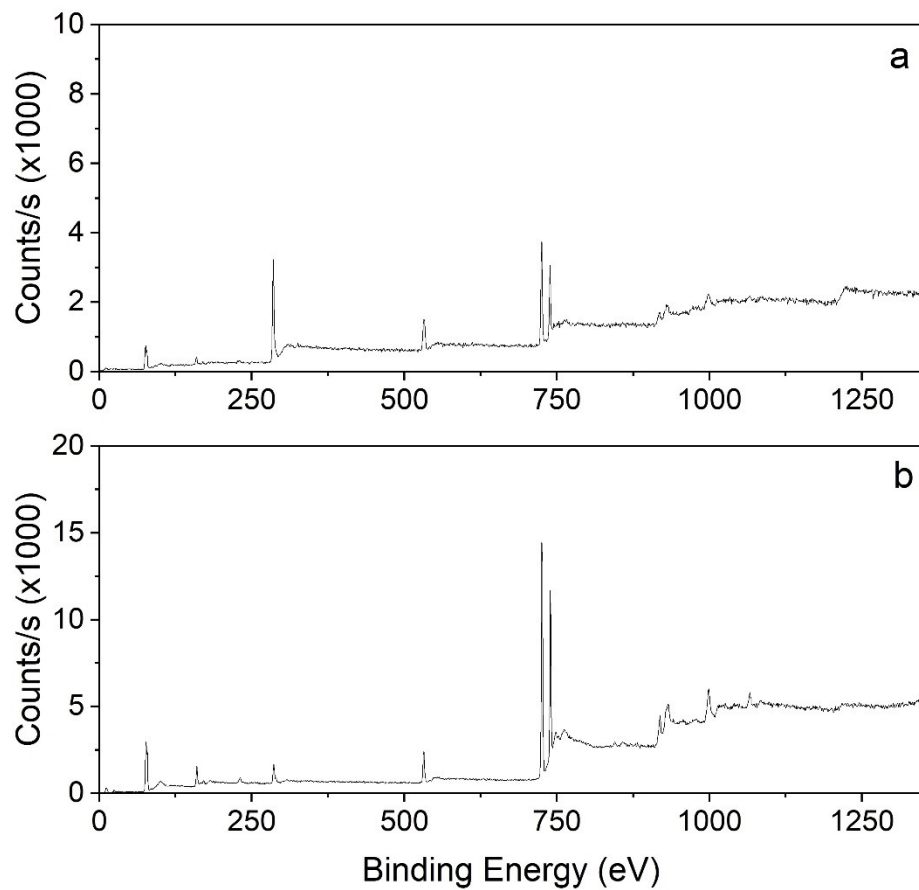


Fig. S20 Survey XPS spectra of (a) Ru/C_exCs (Cs/Ru=10) before, (b) Ru/C_exCs (Cs/Ru=10) before after the reaction testing.

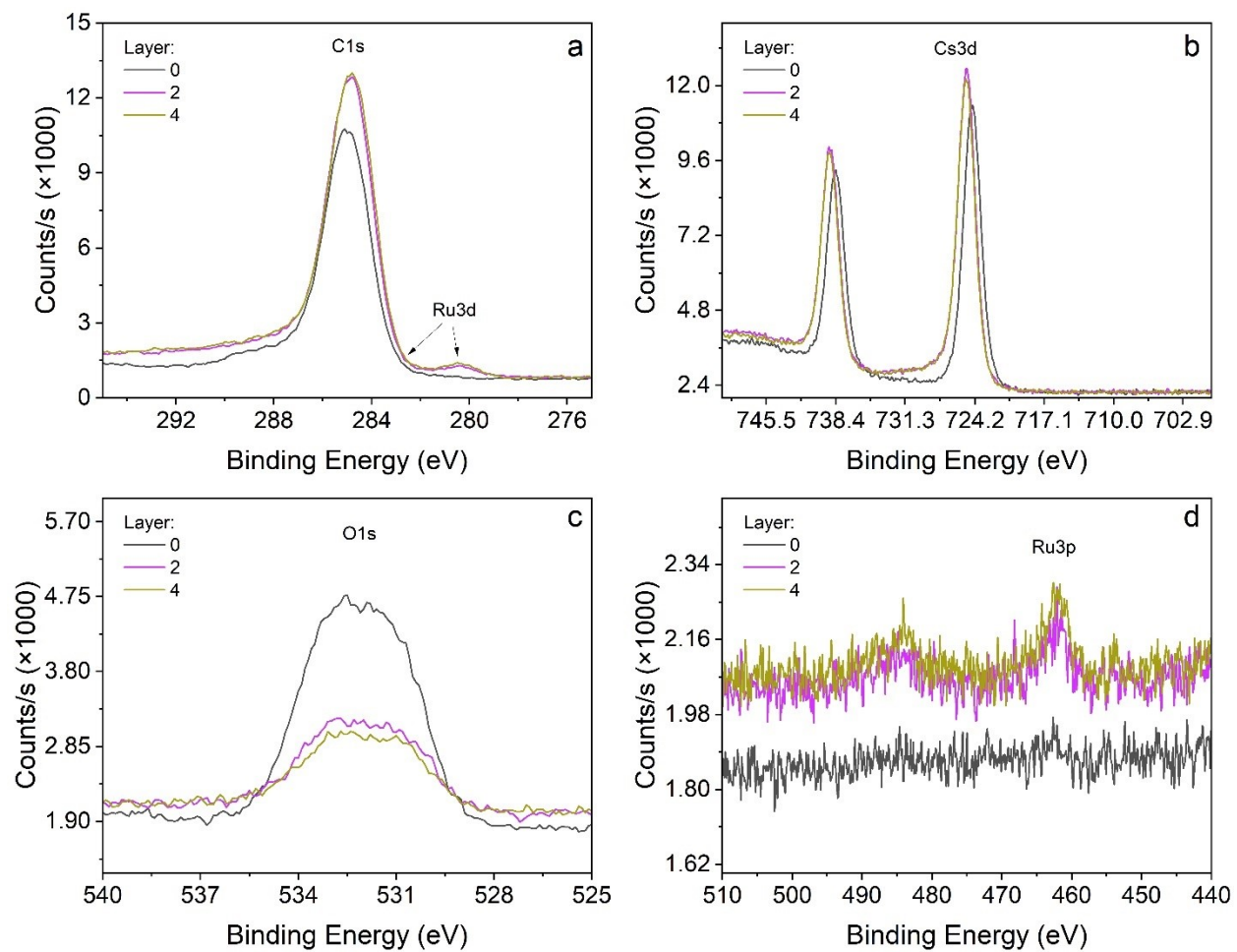


Fig. S21 Detailed XPS spectra of the Ru/C_{ex}Cs (Cs/Ru=10) before reaction testing.

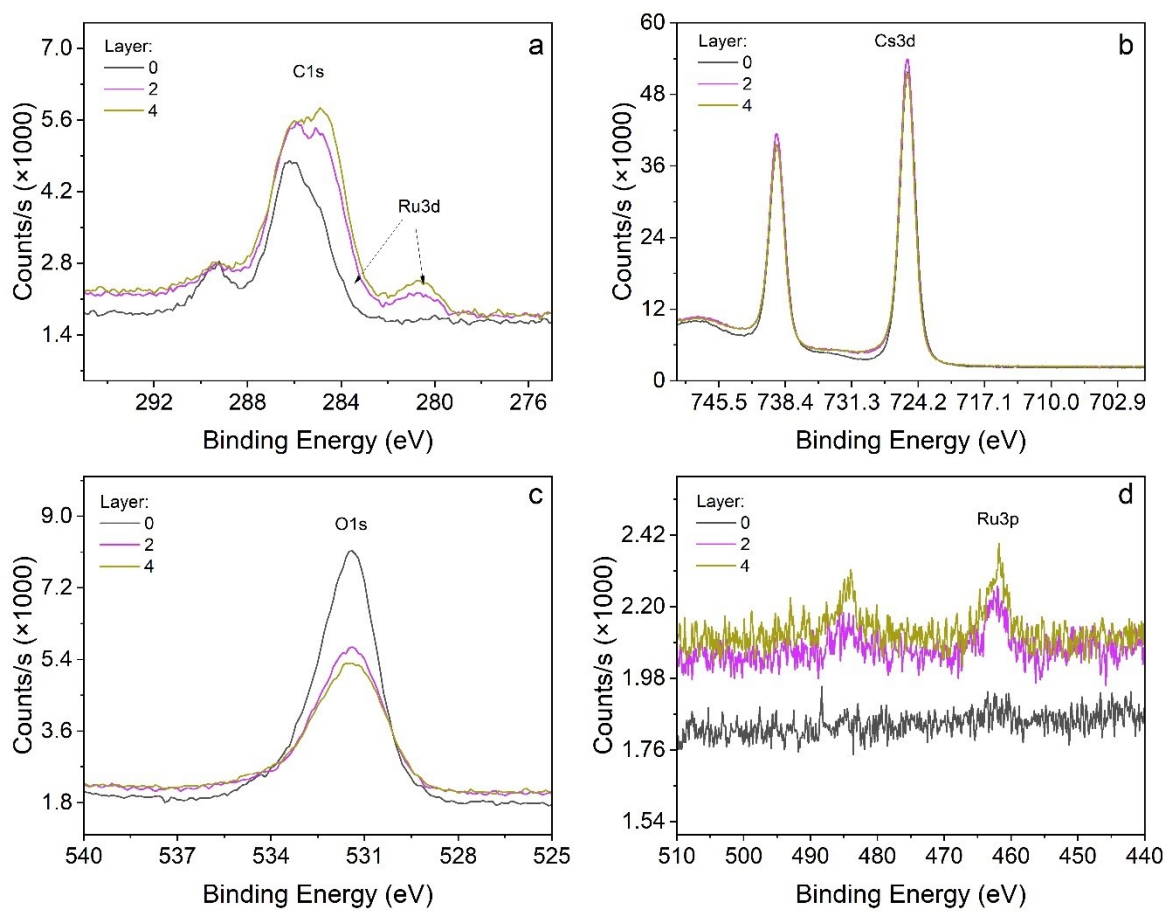


Fig. S22 Detailed XPS spectra of the Ru/C_{ex}Cs (Cs/Ru=10) after reaction testing.

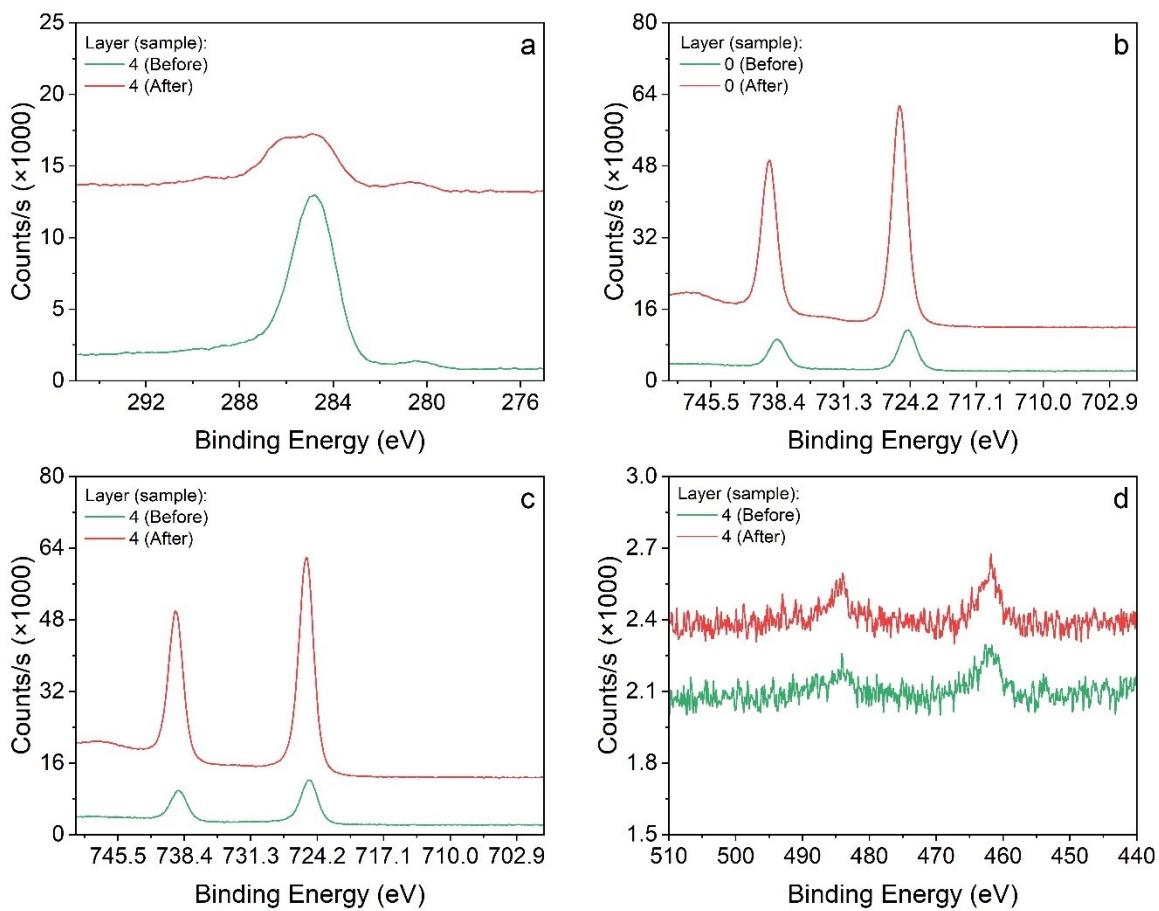


Fig. S23 Stacked detailed XPS spectra of Ru/C_{ex}Cs (Cs/Ru=10) before and after reaction testing.

References:

- 1 J. Zheng, F. Liao, S. Wu, G. Jones, T. Chen, J. Fellowes, T. Sudmeier, I. J. McPherson, I. Wilkinson and S. C. E. Tsang, *Angew. Chemie Int. Ed.*, 2019, **58**, 17335–17341.
- 2 M. Kitano, Y. Inoue, Y. Yamazaki, F. Hayashi, S. Kanbara, S. Matsuishi, T. Yokoyama, S. W. Kim, M. Hara and H. Hosono, *Nat. Chem.*, 2012, **4**, 934–940.
- 3 Z. Ma, S. Zhao, X. Pei, X. Xiong and B. Hu, *Catal. Sci. Technol.*, 2017, **7**, 191–199.
- 4 X. Wang, L. Li, T. Zhang, B. Lin, J. Ni, C.-T. Au and L. Jiang, *Chem. Commun.*, 2019, **55**, 474–477.
- 5 W. Li, S. Wang and J. Li, *Chem. – An Asian J.*, 2019, **14**, asia.201900618.
- 6 B. Lin, L. Heng, B. Fang, H. Yin, J. Ni, X. Wang, J. Lin and L. Jiang, *ACS Catal.*, 2019, **9**, 1635–1644.
- 7 J. Li, W. Wang, W. Chen, Q. Gong, J. Luo, R. Lin, H. Xin, H. Zhang, D. Wang, Q. Peng, W. Zhu, C. Chen and Y. Li, *Nano Res.*, 2018, **11**, 4774–4785.
- 8 Y. Kobayashi, Y. Tang, T. Kageyama, H. Yamashita, N. Masuda, S. Hosokawa and H. Kageyama, *J. Am. Chem. Soc.*, 2017, **139**, 18240–18246.
- 9 P. Wang, F. Chang, W. Gao, J. Guo, G. Wu, T. He and P. Chen, *Nat. Chem.*, 2017, **9**, 64–70.
- 10 K. Sato, K. Imamura, Y. Kawano, S. Miyahara, T. Yamamoto, S. Matsumura and K. Nagaoka, *Chem. Sci.*, 2017, **8**, 674–679.
- 11 H. Cao, J. Guo, F. Chang, C. Pistidda, W. Zhou, X. Zhang, A. Santoru, H. Wu, N. Schell, R. Niewa, P. Chen, T. Klassen and M. Dornheim, *Chem. - A Eur. J.*, 2017, **23**, 9766–9771.
- 12 Z. Ma, X. Xiong, C. Song, B. Hu and W. Zhang, *RSC Adv.*, 2016, **6**, 51106–51110.
- 13 M. Kitano, Y. Inoue, H. Ishikawa, K. Yamagata, T. Nakao, T. Tada, S. Matsuishi, T. Yokoyama, M. Hara and H. Hosono, *Chem. Sci.*, 2016, **7**, 4036–4043.
- 14 W. Gao, P. Wang, J. Guo, F. Chang, T. He, Q. Wang, G. Wu and P. Chen, *ACS Catal.*, 2017, **7**, 3654–3661.

- 15 S. Hagen, R. Barfod, R. Fehrmann, C. J. H. Jacobsen, H. T. Teunissen, K. Ståhl and I. Chorkendorff, *Chem. Commun.*, 2002, **11**, 1206–1207.
- 16 S. Hagen, R. Barfod, R. Fehrmann, C. J. H. Jacobsen, H. T. Teunissen and I. Chorkendorff, *J. Catal.*, 2003, **214**, 327–335.
- 17 J. Li, J. Wu, H. Wang, Y. Lu, T. Ye, M. Sasase, X. Wu, M. Kitano, T. Inoshita and H. Hosono, *Chem. Sci.*, 2019, **10**, 5712–5718.
- 18 Y. Inoue, M. Kitano, M. Tokunari, T. Taniguchi, K. Ooya, H. Abe, Y. Niwa, M. Sasase, M. Hara and H. Hosono, *ACS Catal.*, 2019, **9**, 1670–1679.
- 19 Y. Tsuji, M. Kitano, K. Kishida, M. Sasase, T. Yokoyama, M. Hara and H. Hosono, *Chem. Commun.*, 2016, **52**, 14369–14372.
- 20 Y. Inoue, M. Kitano, K. Kishida, H. Abe, Y. Niwa, M. Sasase, Y. Fujita, H. Ishikawa, T. Yokoyama, M. Hara and H. Hosono, *ACS Catal.*, 2016, **6**, 7577–7584.
- 21 M. Kitano, Y. Inoue, M. Sasase, K. Kishida, Y. Kobayashi, K. Nishiyama, T. Tada, S. Kawamura, T. Yokoyama, M. Hara and H. Hosono, *Angew. Chemie - Int. Ed.*, 2018, **57**, 2648–2652.
- 22 M. Hattori, T. Mori, T. Arai, Y. Inoue, M. Sasase, T. Tada, M. Kitano, T. Yokoyama, M. Hara and H. Hosono, *ACS Catal.*, 2018, **8**, 10977–10984.
- 23 Y. Wu, C. Li, B. Fang, X. Wang, J. Ni, B. Lin, J. Lin and L. Jiang, *Chem. Commun.*, 2020, **56**, 1141–1144.
- 24 F. Chang, Y. Guan, X. Chang, J. Guo, P. Wang, W. Gao, G. Wu, J. Zheng, X. Li and P. Chen, *J. Am. Chem. Soc.*, 2018, **140**, 14799–14806.
- 25 Y. Gong, J. Wu, M. Kitano, J. Wang, T. N. Ye, J. Li, Y. Kobayashi, K. Kishida, H. Abe, Y. Niwa, H. Yang, T. Tada and H. Hosono, *Nat. Catal.*, 2018, **1**, 178–185.
- 26 L. Li, T. Zhang, J. Cai, H. Cai, J. Ni, B. Lin, J. Lin, X. Wang, L. Zheng, C. T. Au and L. Jiang, *J. Catal.*, 2020, **389**, 218–228.
- 27 T. N. Ye, S. W. Park, Y. Lu, J. Li, M. Sasase, M. Kitano and H. Hosono, *J. Am. Chem. Soc.*,

- 2020, **142**, 14374–14383.
- 28 T. N. Ye, S. W. Park, Y. Lu, J. Li, M. Sasase, M. Kitano, T. Tada and H. Hosono, *Nature*, 2020, **583**, 391–395.
- 29 K. Sato, S. ichiro Miyahara, Y. Ogura, K. Tsujimaru, Y. Wada, T. Toriyama, T. Yamamoto, S. Matsumura and K. Nagaoka, *ACS Sustain. Chem. Eng.*, 2020, **8**, 2726–2734.
- 30 Q. Wang, J. Pan, J. Guo, H. A. Hansen, H. Xie, L. Jiang, L. Hua, H. Li, Y. Guan, P. Wang, W. Gao, L. Liu, H. Cao, Z. Xiong, T. Vegge and P. Chen, *Nat. Catal.* 2021 411, 2021, **4**, 959–967.
- 31 F. Rosowski, A. Hornung, O. Hinrichsen, D. Herein, M. Muhler and G. Ertl, *Appl. Catal. A Gen.*, 1997, **151**, 443–460.